Eddy formation by dense flows on slopes in a rotating fluid

By GREGORY F. LANE-SERFF[1] and PETER G. BAINES[2]

[1] Department of Oceanography, University of Southampton, Southampton Oceanography Centre, Southampton SO14 3ZH, UK

[2] Division of Atmospheric Research, CSIRO, PB1, Mordialloc, Victoria 3195, Australia

Properties of the flow generated by a continuous source of dense fluid on a slope in a rotating system are investigated with a variety of laboratory experiments. The dense fluid may initially flow down the slope but it turns (under the influence of rotation) to flow along the slope, and initial geostrophic adjustment gives it an anticyclonic velocity profile. Some of the dense fluid drains downslope in a viscous Ekman layer, which may become unstable to growing waves. Provided that the viscous draining is not too strong, cyclonic vortices form periodically in the upper layer and the dense flow breaks up into a series of domes. Three processes may contribute to the formation of these eddies. First, initial downslope flow of the dense current may stretch columns of ambient fluid by the 'Taylor column' process (which we term 'capture'). Secondly, the initial geostrophic adjustment implies lower-layer collapse which may stretch the fluid column, and thirdly, viscous drainage will progressively stretch and spin up a captured water column. Overall this last process may be the most significant, but viscous drainage has contradictory effects, in that it progressively removes dense lower-layer fluid which terminates the process when the layer thickness approaches that of the Ekman layer. The eddies produced propagate along the slope owing to the combined effects of buoyancy–Coriolis balance and 'beta-gyres'. This removes fluid from the vicinity of the source and causes the cycle to repeat. The vorticity of the upper-layer cyclones increases linearly with $\Gamma = L\alpha/D$ (where L is the Rossby deformation radius, α the bottom slope and D the total depth), reaching approximately $2f$ in the experiments presented here. The frequency at which the eddy/dome structures are produced also increases with Γ, while the speed at which the structures propagate along the slope is reduced by viscous effects. The flow of dense fluid on slopes is a very important part of the global ocean circulation system and the implications of the laboratory experiments for oceanographic flows are discussed.

1. Introduction

The flow of dense water from marginal seas or through sills down into the deep ocean is an important part of the global thermohaline circulation. Examples include the flow of dense water formed in the polar regions down into the surrounding oceans (see Baines & Condie 1997 for a review of the Antarctic situation) and also smaller-scale flows such as Mediterranean water flowing into the Atlantic and the flow through the Bass Strait into the Tasman Sea. These complex flows are poorly resolved in present ocean circulation and climate models, yet they are crucial to the long-term behaviour of the global ocean system (see, for example, Harvey 1996).

There have been a number of models of dense plumes on slopes using averaged or

integral properties to describe the plume. For example, Smith (1975), Killworth (1977) and Price & Baringer (1994) use 'streamtube' models to investigate the flow of a dense current on a slope in a rotating system. In such models the plume is assumed to follow a path described in terms of the plume centreline. At each position along the path the plume properties are given in terms of steady time-averaged velocities and densities, with the cross-sectional shape of the plume given in terms of some width and height scales. The engulfing of ambient fluid into the plume is generally parametrized using an entrainment constant, relating the velocity of ambient fluid into the plume to the local velocity scale within the plume (more sophisticated models include the stabilizing effect of buoyancy, e.g. Price & Baringer). Drag and buoyancy forces are also treated in an integral or averaged fashion. In these models the plume flow is basically alongslope, but with the plume taken slightly downslope by the effects of viscosity. The volume flux in the plume grows because of entrainment, which also results in a steady reduction in the density difference between the plume and the ambient fluid as one moves along the plume. Where ambient stratification is included this results in the plume eventually reaching a neutral level, where it has the same density as the ambient seawater.

Similar models have been developed for non-rotating two-dimensional currents on slopes (Jenkins 1991; Lane-Serff 1993, 1995; Bombosch & Jenkins 1995). Some of these models include extra effects such as the melting and freezing of ice to simulate flows under ice shelves. Baines (1997) has performed laboratory experiments of non-rotating downslope flows in a stratified fluid. These experiments show that a simple entrainment model is not appropriate where the ambient fluid is stratified. In addition to entrainment of ambient fluid into the current, detrainment of fluid from the plume is observed, and this detrained fluid then mixes with the ambient fluid.

The flow of dense fluid released on a horizontal surface (or light fluid on an upper surface) in a rotating system has been reviewed by Griffiths (1986). When the release is against a wall the dense fluid flows as a gravity current along the wall with a width that scales on the Rossby deformation radius (see §3). A number of workers have used laboratory experiments to investigate dense flows on a slope in a rotating system. Mory, Stern & Griffiths (1987) produced coherent eddies by releasing a volume of dense fluid onto a sloping bottom. A strong cyclonic eddy was formed in the water column above the dense fluid and the entire system moved 'north-westwards' (i.e. along- and upslope), though some of the dense fluid drained downslope in a viscous Ekman layer. Whitehead *et al.* (1990) conducted a variety of experiments investigating flows generated by continuous sources. These flows were observed to produce a train of eddies under certain conditions. The stability of bottom currents on a slope with a deep upper layer has been described by Griffiths, Killworth & Stern (1982), and with an active upper layer by Swaters & Flierl (1991) Swaters (1991, 1993 *a, b*) and Karsten & Swaters (1996).

The first quantitative experiments on downslope flows in rotating systems were by Smith (1977), who released fluid continuously from a localized source on an axisymmetric slope. For the parameter range of the experiments, eddies were produced in virtually all circumstances. Smith also identified the viscous drainage layer, gave a theoretical framework for the extinguishment of the inviscid current, and showed that this was consistent with his experiments. He compared the observed frequency of eddy production with predictions from two-layer baroclinic instability theory, and found that the frequency showed a similar trend with current speed, but otherwise the agreement was generally poor. Nagata *et al.* (1993), Condie (1995) and Zatsepin, Kostyanoi & Semenov (1996) conducted axisymmetric experiments with dense fluid

flowing radially out of a source at the top of an axisymmetric hill (e.g. a truncated cone). Viscous effects were very important in most of these experiments, with a significant Ekman layer. An important result from these studies is that the downslope component of the flow occurs in a thin viscous boundary layer with a maximum thickness that scales on the Ekman layer thickness and a velocity that is given by a balance between Coriolis and gravitational accelerations (this is discussed further in §3). Whitehead *et al.* (1990), Nagata *et al.* and Zatsepin *et al.* all note the occasional presence of waves on this viscous downslope flow. The rest of the flow is confined to an essentially inviscid alongslope geostrophic current. In addition to an axisymmetric source, Nagata *et al.* examine flow from a horizontal line source, and Condie presents a few results from experiments where the source is a channel releasing fluid at one point on the hill.

Here we present the results of a comprehensive set of experiments investigating the flow of dense water from a steady localized source. We use a number of slope angles and a wide range of rotation rates, density differences and ambient fluid depths, but the ambient fluid is always uniform (unstratified).

The experiments are described in detail in the next section. In §3 we examine the appropriate scalings for this type of flow. The results of the experiments are presented in §4 and in §5 we discuss eddy formation and applications to oceanographic flows. In the final section we summarize the work and outline future studies.

2. Experiments

The apparatus is shown in figures 1 and 2. Two tanks were used: a glass tank with base 75 cm × 75 cm and height 70 cm, and a Perspex tank with a circular base of diameter 95 cm and height 50 cm. Slopes were placed in the tanks, with a horizontal 'shelf' at the top of the slope. The slopes did not extend to the edges of the tanks, so that dense fluid could cascade off the slopes and not interfere with the later flow. Dense fluid was introduced over a weir (7–10 cm wide and 1–2 cm high) at the top of the slope. Except for the section occupied by the weir, the shelf was separated from the slope by a vertical barrier. Two simple plane slopes (angles 5.7° and 15.7° from the horizontal) were used in the square tank and a truncated cone (slope 13.8° from the horizontal) was used in the circular tank. The cone had a small sector removed, to allow fluid that had flowed all the way around the slope to cascade down below the slope, and a radial barrier, to reduce secondary motions induced by the cascading dense fluid.

The tanks were filled with fresh water from a mains supply. Denser fluid was made by adding common salt, with densities measured using an Anton Paar densitometer. The dense fluid was marked by adding vegetable dye and placed in a bucket mounted on the rotating table superstructure. For most of the experiments the dense fluid was introduced via a flowmeter into a channel on the shelf at the top of the slope. The relative density difference between the source fluid and the ambient fluid was in the range 0.01 to 0.15 and flow rates were from 20 to 35 cm³ s⁻¹. An L-shaped channel was used in the square tank, a straight channel in the circular tank. The channels contained some mesh to help smooth the flow. The dense fluid then flowed over the weir, giving a steady source flow onto the slope (see figure 2).

In order to test the sensitivity of the results to the initial conditions, a number of experiments in the circular tank were conducted with a different type of source. For these experiments the dense fluid was injected horizontally along the slope through a nozzle (of approximately inverted parabolic shape, with a central height of 1.5 cm and
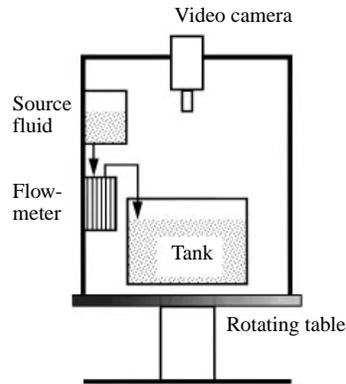
FIGURE 1. Sketch showing the arrangement of the apparatus on the rotating table.

a width of 10 cm) mounted on the upper part of the slope. This source is also more convenient for theoretical discussion (see §5).

The Earth's rotation was simulated by placing the tanks on a belt-driven rotating table which has a 1.1 m diameter platter, controlled by a tacho-feedback system. The rotation rate of the table was calculated by measuring the time for a number of rotations (typically ten) using a stopwatch. The range of rotation rates used was from 20 down to 3 s per revolution ($f = 0.63$ to 4.2 s^{-1}). The sense of the rotation was always clockwise, when viewed from above ('southern-hemisphere').

The centrifugal acceleration caused by the rotation results in curvature of the free surface so that it (and other isopotential surfaces) becomes parabolic in shape. This has the effect of adding a parabolic hill to the bottom topography. (This effective parabolic hill is the only topography present in the experiments of Condie 1995.) This merely increases the slope in the circular tank (with the slope increasing with increasing radius) but it makes the effective topography in the square tank more complicated (a combination of plane slope and parabolic hill). The magnitude of the effective extra slope (which varies with position) has generally been kept significantly smaller than the real slope in our experiments (typically 10% or less), but there are a couple of rapidly rotating experiments where this effect approaches 40% at positions furthest from the centre of rotation. The weir was modified so that its crest was approximately level with respect to the local isopotential surface.

The experiments were filmed using a U-matic video system with a camera placed on the rotating table, viewing the apparatus from above to give a plan view. A grid was marked on the slope to facilitate taking measurements from the video recordings.

The procedure for each experiment was as follows. The tank was filled to the required depth with fresh water and the bucket filled with salt solution and dye (with samples taken to check the densities). The table was then rotated at the desired rate and the water in the tank allowed to spin up to solid-body rotation (taking typically 20 min). The flow of dense fluid was started and the flow rate noted. The flow rate usually decreased slowly (by up to 10%) during the course of the experiment. The duration of the dense flow was typically 3 to 5 min.

Here we present the results from a total of 88 experiments, 40 in the square tank (28 with the 15.7° slope and 12 with the 5.7° slope) and 48 in the circular tank (of which 22 use the source mounted on the slope). The parameters for the experiments are given in table 1, which is not reproduced here, but is available from the authors or the JFM Editorial Office.

FIGURE 2. Schematic sections and plans of the two tanks used: (*a*) the square tank, (*b*) the circular tank, and (*c*) the source used for injecting fluid along the slope in some experiments. The position of this alternative source is indicated in (*b*).

3. Scalings

An experiment with a large depth of ambient fluid above the shelf (more than 30 cm) is shown in figure 3. The dense fluid flows over the weir in a layer that is deeper on the left (looking downstream). The flow is initially downslope but turns left (recall that southern hemisphere rotation was used) and much of the flow moves alongslope in a current confined to the upper part of the slope. However, some of the fluid flows at an angle downslope in a thin layer. Under some conditions this layer develops waves as it moves down the slope.

For most of the experiments the width of the weir was wider than the Rossby radius so that the flow was not restricted there. Where the width of the weir restricts the flow we expect the flow to undergo a more complicated adjustment, but in any case the flow has adjusted and set its own width, depth and velocity scales rather than having these preset at the source. This self-adjustment is how many naturally occurring dense flows behave and we base our scalings on this process. First, we consider the flow of an inviscid dense current on a semi-infinite horizontal surface bounded by a vertical wall, with the current flowing along the wall and having an approximately triangular cross-section (see, for example, Griffiths & Hopfinger 1983). If the height of the current is given by d, then the width of the current will scale with the Rossby deformation radius

$$L = (g'd)^{1/2}/f, \tag{1}$$

where $g' = (\Delta\rho/\rho)\,g$ is the reduced gravity and f is the Coriolis parameter. The velocity in the current will be given from a standard gravity current model as

$$u \sim (g'd)^{1/2}. \tag{2}$$

The volume flux of the current will then be given by

$$Q \sim \tfrac{1}{2}dLu. \tag{3}$$

The parameters that are set externally are g', f and Q, with the flow adjusting in response. This gives our estimates of the appropriate height, width and velocity scales as

$$d = (2Qf/g')^{1/2}, \tag{4}$$

$$L = (2Qg')^{1/4}f^{-3/4}, \tag{5}$$

and

$$u = (2Qfg')^{1/4}. \tag{6}$$

These scales are for an inviscid flow on a horizontal surface. For flow on a slope it is useful to introduce another velocity scale. If an isolated volume of dense fluid is moving along the slope (with uphill being to the left in the southern hemisphere) the Coriolis acceleration will be upslope while the gravitational acceleration will be downslope. The alongslope speed for which these accelerations balance is given by

$$c_N = g'\alpha/f, \tag{7}$$

where α is the (small) angle of the slope from the horizontal. This speed is also known as the 'Nof speed' (e.g. Swaters & Flierl 1991). Nagata *et al.* (1993) showed (for an axisymmetric flow) that the maximum thickness of the viscous draining layer scaled on the Ekman layer thickness,
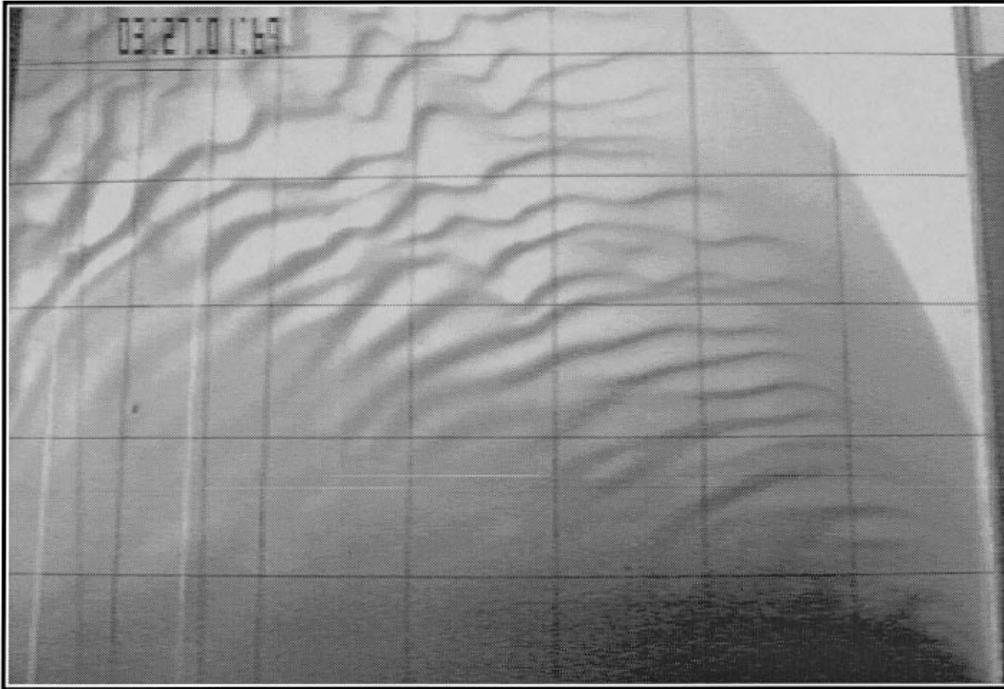
$$d_\nu = (2\nu/f)^{1/2}, \tag{8}$$

FIGURE 3. Digitized video image of a plan view of an experiment in the square tank, 15.7° slope, with a deep layer of ambient fluid, $D = 33.5$ cm, above the dark, dense current (run 21: rotation rate = 6 s/rev, $Q = 26$ cm^3 s^{-1}, $g' = 51.0$ cm s^{-2}). The source of the dense fluid is just below the bottom right-hand corner of the image. The dense current mostly flows from right to left along the top of the slope (the bottom edge of the image) but with some fluid draining at an angle down the slope. While the alongslope flow is smooth, the downslope flow develops a series of waves with crests approximately perpendicular to the local flow direction. The square grid is spaced at 10 cm and two strings (see figure 6) are visible towards the left of the image. The triangular dark region on the right-hand edge of this and the next figure is the sidewall of the tank.

where ν is the kinematic viscosity (taken here to be 0.01 cm^2 s^{-1}). They also showed that the velocity in this layer scaled on c_N. Thus we can introduce an alongslope lengthscale: the distance over which the initial flux is drained,

$$Y = (Qf^{3/2})/(g'\alpha(2\nu)^{1/2}). \tag{9}$$

(A very similar drainage scale distance was identified by Smith 1977.) At distances short compared with Y we expect viscous effects to be unimportant, with viscous effects becoming significant at distances of order Y and larger (though even a small amount of drainage may have a significant affect on the vorticity by stretching fluid columns). The relative importance of the viscous draining can be quantified in terms of the ratio of the alongslope draining distance to the width of the flow,

$$Y/L = 2^{-3/4} Q^{3/4} f^{9/4} \nu^{-1/2} g'^{-5/4} \alpha^{-1}. \tag{10}$$

The parameters for the experiment shown in figure 4 are similar to those for the experiment in figure 3, except that the depth of the ambient fluid above the shelf is smaller (approximately 9 cm). In this case the alongslope flow breaks up, with strong cyclonic eddies observed in the ambient fluid and domes of dense fluid moving along the slope. The wall at the top of the slope may restrict any upslope movement of the
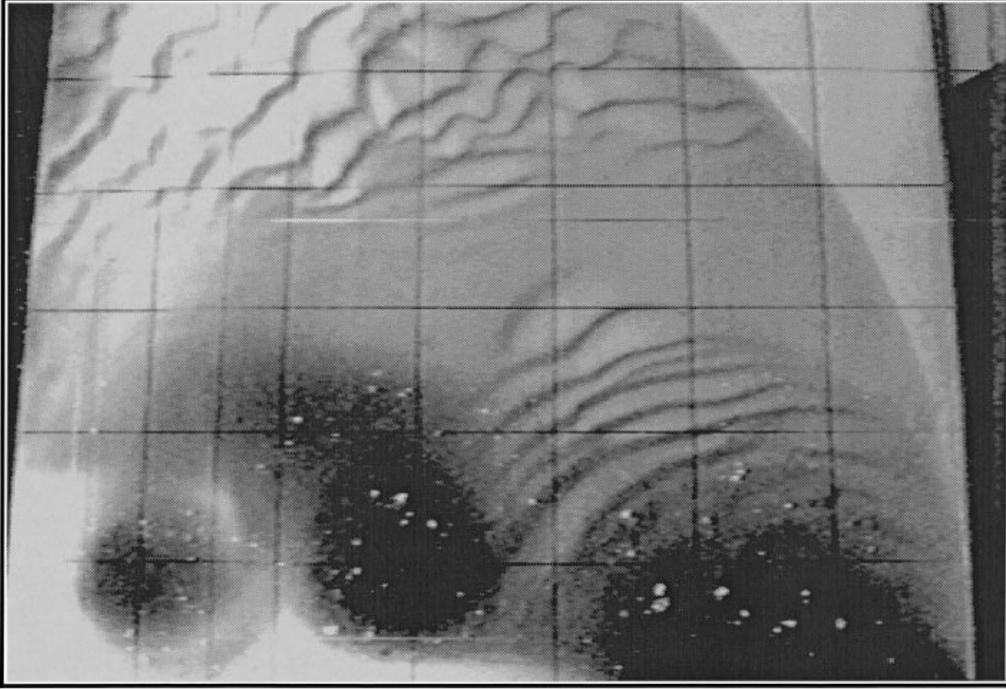
FIGURE 4. Similar to figure 3 but with a shallow depth of ambient fluid ($D = 8.7$ cm) above the dense current (run 23: $Q = 28$ cm^3 s^{-1}, $g' = 49.0$ cm s^{-2}). The dense flow has now broken up into a series of isolated domes with strong cyclonic vortices in the overlying fluid. The strength of the downslope flow, and the presence of waves on this flow, is affected by the eddies. The waves near the bottom of the slope (top of the image) are associated with the central eddy.

domes. If we assume that the domes of dense fluid under the eddies are cylinders with a height and radius given by equations (4) and (5) then the time for the flux Q to fill each dome is $2\pi/f$, which is the time for one half-revolution of the table.

Eddy formation occurs when the depth of the ambient fluid is small, suggesting that it is related to vortex stretching in the fluid above the current. The current initially flows downslope a distance that scales on the Rossby radius before it turns and flows alongslope (for the weir flows). If we assume that the current takes the ambient fluid above it out into deeper water then we see that the ambient fluid is stretched by an amount $L\alpha$. This, compared with the initial height of the ambient fluid columns, give the relative stretching as

$$\Gamma = L\alpha/D, \tag{11}$$

where D is the depth of the ambient fluid above the incoming current.

A number of other parameters have been introduced in investigations of dense flows on slopes. The basic scaling for the height and width of the current gives a 'geostrophic' slope,

$$S = d/L = (2Qf^5/g'^3)^{1/4}, \tag{12}$$

which can be used to scale the topographic slope, i.e. $s = \alpha/S$. This is also equal to the ratio between the speeds u and c_N, and so in turn is equal to the ratio between the inertial radius for a fluid particle released on a slope ($R_i = c_N/f$) and the Rossby radius, L, that we introduced earlier,

$$s = \alpha/S = c_N/u = R_i/L. \tag{13}$$

From the equations for the flow of a dense current on a slope in a stationary homogeneous environment (e.g. Condie 1995) it can be shown that the current is bi-directional if

$$f^2 d_0 / g' \alpha^2 > 1, \tag{14}$$

and unidirectional otherwise, where d_0 is defined by the potential vorticity of the dense fluid, f/d_0. If we identify d_0 with d, (14) is equivalent to $s < 1$ where s is defined by (13). A current on a 'steep' topographic slope can have a cross-sectional shape whose slope (i.e. d_x) is everywhere negative (supporting unidirectional flow), while on a 'shallow' slope the current slope must have both signs.

In his investigation of the stability of alongslope currents, Swaters (1991) introduces an interaction parameter, μ. This parameter incorporates a Rossby radius based on the depth of the ambient fluid

$$R = (g'D)^{1/2}/f, \tag{15}$$

which may be compared with equation (1). With the current depth given by our standard scaling, the Swaters interaction parameter is

$$\mu = d/(R\alpha) = (1/s)(d/D)^{1/2}. \tag{16}$$

We use the scales introduced in this section in our analysis of the results of the experiments.

4. Results

We will first describe the results for those experiments where the dense fluid flowed over a weir at the top of the slope. The flows where the dense fluid was injected along the slope are described towards the end of this section.

4.1. *Basic features*

On leaving the source the flow turns under the influence of rotation. The flow is then observed to have two main components: an inviscid alongslope flow and a viscous, draining, downslope flow. Under certain conditions the alongslope flow is not continuous but is made up of a series of dense domes, with cyclonic eddies formed in the ambient fluid above the domes. The domes are formed very close to the source and then propagate along the slope with, in some cases, some small upslope velocity (though upslope flow is impeded by the vertical wall at the top of the slope). The downslope excursion of the flow (before turning to flow along the slope) was estimated for a few images from some of the experiments either from the position of the centre of eddies (when these were formed) or from the apparent centreline of the alongslope flow. For those flows which broke up, the size of the dome/eddy structures was also estimated. These results are plotted in figure 5. There is a good deal of scatter, in part because of the subjective nature of the measurements, and the results should be treated with caution. We conclude that the lengths scale on L, but a wider range of Rossby radii would be needed to test this convincingly (requiring a larger tank). Assuming this linear scaling, the downslope excursion is found to be $(2.3 \pm 0.1)\, L$ and the eddy radius $(1.25 \pm 0.05)\, L$.

The depth of the dense fluid was found in a few places in some experiments by using a piece of string with one end taped to the slope near to its bottom edge and the other end attached a known distance up the wall at the top of the slope. The depth at the point where the string passes into the current can then be calculated (see figure 6). The depth of the dense layer can also be estimated from the video images (the image is
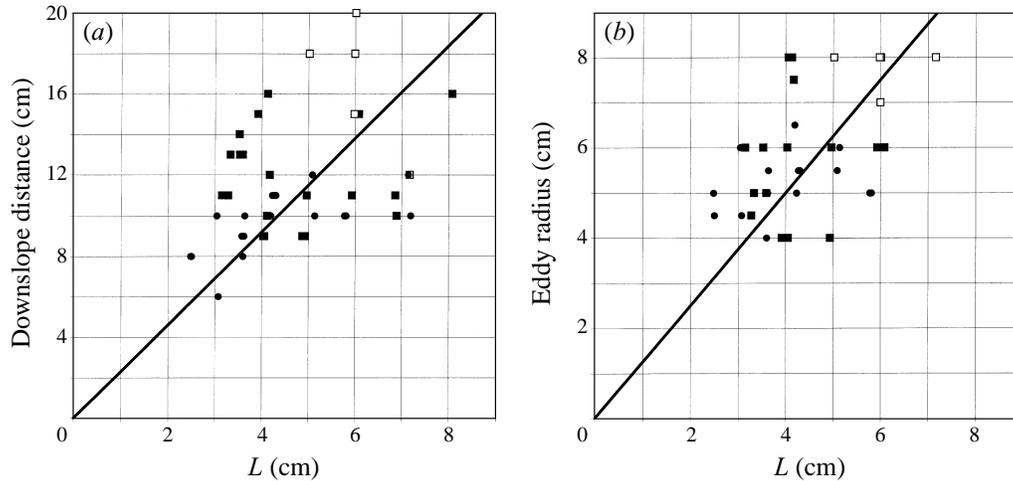
FIGURE 5. (*a*) Downslope excursion and (*b*) eddy radius as functions of the Rossby radius, L. The best-fit lines through the origin are also plotted, (*a*) $(2.3 \pm 0.1) L$ and (*b*) $(1.25 \pm 0.05) L$. ■, Square tank, $15.7°$ slope; □, square tank, $5.7°$ slope; ●, circular tank, $13.8°$ slope.
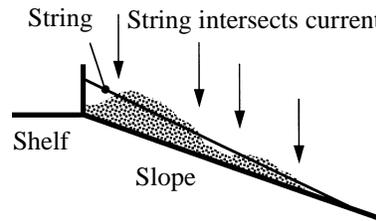

FIGURE 6. A sketch showing how lengths of string, attached between a point near the bottom of the slope and the wall at the top of the slope, were used to estimate the thickness of the dense flow.

darker where the dense flow is deeper) and the relationship between layer thickness and light intensity can be calibrated at a few points using the string method. Some video images were digitized and processed using the DigImage system, and an example is shown in figure 7. As figure 7 shows, the dense domes are not perfectly regular in shape. The presence of the dome/eddy structures also has an effect on the viscous downslope flow, modulating its strength (with the layer thickest downslope of the eddies), and thus the waves that develop on this flow are most prominent there.

In addition to dyeing the dense fluid, in some experiments the surface was sprinkled with small floating particles or powder to identify motions in the ambient fluid. The centres of the eddies in the ambient fluid did not always appear to lie directly over the centres of the domes but generally seemed to lag behind the dome. We did not make any direct measurements of the flow within the dense domes, but inferred that it was anticyclonic with respect to the upper part of the eddy. The formation of strong eddies in the water column above the current is a very striking feature of the flow. In the rest of this section we examine the conditions under which the eddies form and the properties of the eddies. The flows were analysed by studying the video recordings of the experiments. The positions of the domes or eddies were estimated by eye, with times being available from a timer display recorded on the video (with a resolution of 0.01 s).
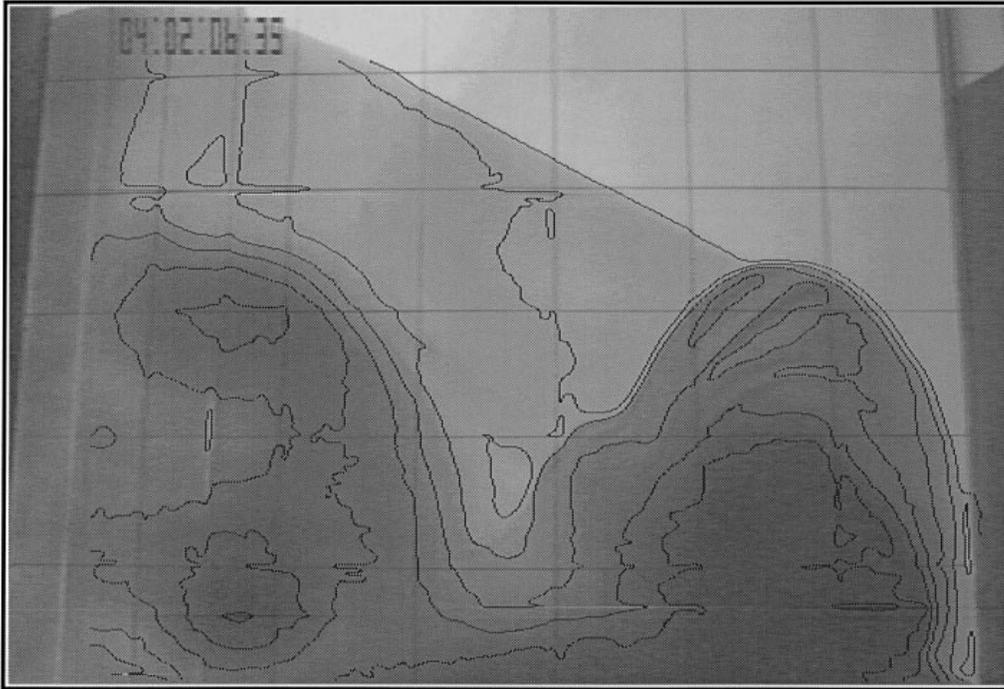
FIGURE 7. A processed image from an experiment (run 26: rotation rate = 6 s/rev, $Q = 27$ cm³ s⁻¹, $D = 8.5$ cm) with the thickness of the flow estimated from the image intensity. The contours are at intervals of approximately 1.1 mm. In this experiment the downslope flow is strongly modulated by the instabilities, with very little flow in between them. Downslope of the right-hand dome/eddy there is a suggestion of two or three short wave crests in the draining flow. However, the draining flow downslope of the left-hand eddy is concentrated in a single feature that is nearly as thick as the dome.

4.2. *Eddy speeds*

The speed of propagation of each eddy along the slope was calculated by using a linear fit to a plot of eddy position against time. The end regions, influenced by the source and the slope edge, were ignored in this fit so that speeds were estimated for a central position along the slope some nominal distance from the source (at $y = 30$ cm from the source for the square tank, 40 cm for the circular tank). The determination of the position of the eddies is somewhat subjective, and there is considerable variation in the speeds of different eddies from the same experiment, so that the typical error bound on our speed estimates is $\pm 15\%$.

The ratio Y/L gives an indication of the importance of viscous effects. As can be seen in figure 8, significant viscous draining results in slower eddies, and sufficient draining prevents the formation of eddies altogether (presumably because all of the dense fluid immediately drains downslope). The best-fit power law curve (to the weir experiments), excluding large values of Y/L (greater than 70), gives

$$c/c_N = (0.10 \pm 0.02)\,(Y/L)^{0.62 \pm 0.06}. \qquad (17a)$$

As Y/L increases, the speed of the eddies (compared with c_N) increases, apparently without limit. Large values of Y/L generally correspond to small values of s, so that the slope may not be important for these flows. The eddies in these cases are more likely to be associated with the instabilities observed in rotating gravity currents on a flat
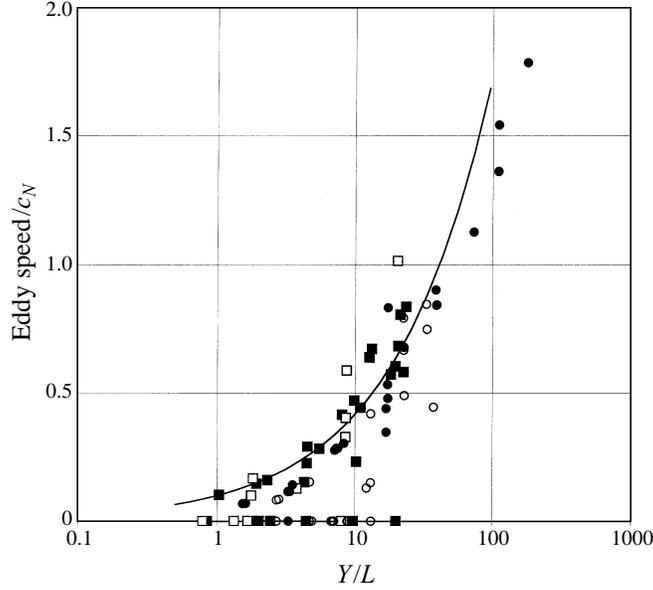
FIGURE 8. Eddy speed (non-dimensionalized with respect to the speed c_N) as a function of the ratio of the draining distance to the current width. Where the eddy speed could not be calculated, the speed is plotted as 0. Two cases not shown here (both in the circular tank) had $Y/L = 1305$ and 383, and speed $= 7.33c_N$ and $3.43c_N$, respectively. A simple power law curve is fitted to the data, excluding large values of Y/L (greater than 70), giving $(0.10 \pm 0.02)(Y/L)^{0.62 \pm 0.06}$. $\bigcirc$, Circular tank injected source; other symbols as figure 5.

surface. Indeed, while the eddy speed is not limited by c_N, the eddy speeds are always less than $0.5u$ (where u is the scale for gravity current speeds from equation (6)). While the velocity scale u is clearly important, we could find no significant relations between the propagation speed scaled with u (i.e. c/u) and any other parameter.

4.3. *Vortex stretching*

Figure 8 shows that eddies are sometimes absent even when we would not expect viscous draining to be significant. In all these cases the stretching parameter, Γ, was small. We did not find a relation between the speed of the eddies and Γ, but there is a clear relation between the frequency of the eddies and the amount of vortex stretching (figure 9). The effect of the eddies on the viscous flow (modulating the waves) was used in determining the eddy frequency, in addition to the direct measurements of the eddies. The production of eddies is more regular than their speed, and the error in the frequency measurements we estimate at $\pm 5\%$ (for most cases). The largest uncertainties occurred for flows where few or no clear eddies could be seen and a frequency could only be estimated from a regular modulation of the viscous flow.

From figure 9 we see that the time interval, T_{int}, between one eddy and the next reduces as Γ increases. The best-fit curve (to the weir flow experiments) of the form reciprocal with offset is

$$T_{int}/T = (0.19 \pm 0.02)/\Gamma + (2.4 \pm 0.2), \tag{17b}$$

where T is the rotation period. Thus the limiting frequency, as stretching increases, is approximately one eddy every two and a half revolutions. Where Γ is very small, no
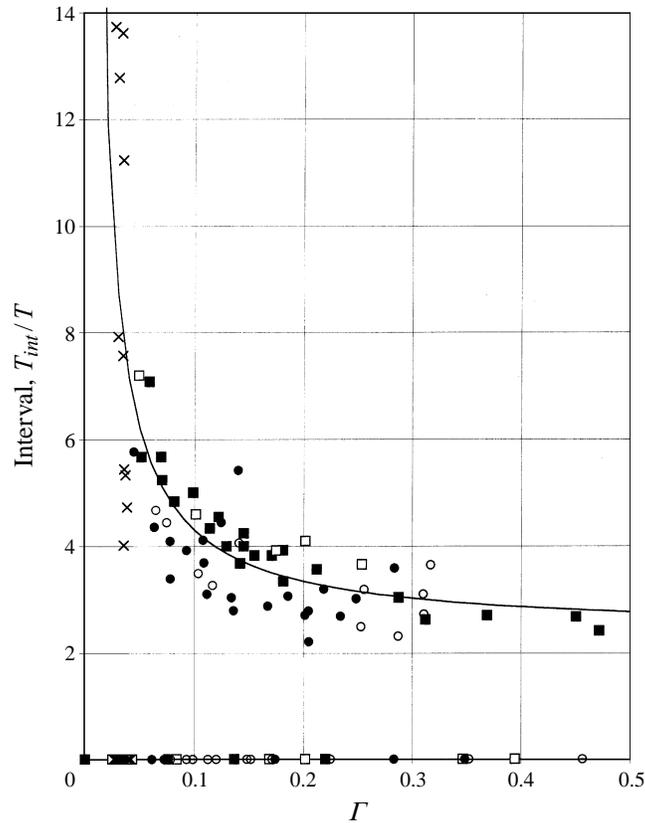
FIGURE 9. The interval between one eddy and the next as a function of the stretching parameter. Where no interval could be calculated, it is plotted as 0. A curve of the form reciprocal with offset is fitted to the (non-zero) data, giving $(0.19 \pm 0.02)/\Gamma + (2.4 \pm 0.2)$. Data from Smith (1977) are also plotted ($\times$). Other symbols as figure 8.

clear frequency could be measured in these experiments. However, results from the series 2 experiments of Smith (1977) are compatible with the present experiments, though the source conditions are somewhat different (flow through a tube rather than over a weir) and the source fluid is significantly more viscous than the ambient fluid. The Smith experiments lie in the small-Γ range and are plotted in figure 9, showing an extension of the above relationship to smaller Γ.

4.4. *Eddy formation*

In figure 10 the parameter ranges covered by the weir experiments (in terms of Y/L and Γ) are displayed. The plot is divided into three regions: (i) a region in which all the experiments produced a number of clear eddies whose speed and frequency could be determined, (ii) a region which produced no eddies or even any measurable regular oscillation in the flow, and finally (iii) an overlap region. The overlap region includes experiments that produced clear eddies, experiments that produced no eddies and experiments for which either the speed or the frequency of eddies could not be determined. We see that provided there is sufficient stretching ($\Gamma > 0.07$, in our experiments) and provided there is not too much viscous draining ($Y/L > 3.5$) then a regular series of cyclonic eddies is observed in the ambient fluid.
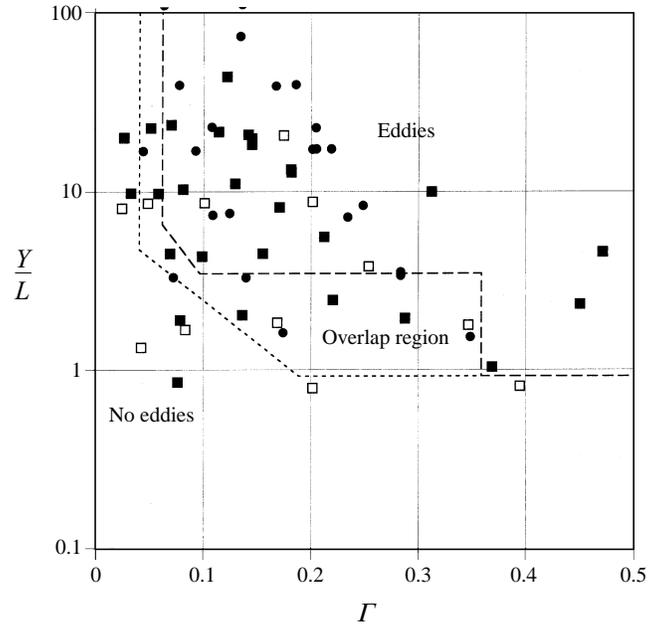
FIGURE 10. The parameter space covered by the experiments showing the region where eddy formation occurred. Symbols as figure 5.

4.5. *Eddy strength*

The flow in the ambient fluid was estimated by observing particles or powder scattered on the surface of the water. Particles were observed to enter and leave the eddy system, so that it is apparent that the eddy does not consist of a translating column of fluid. The eddy structure moves through the ambient fluid, though fluid nearer the centre of the eddy appears to be trapped in the eddy for a longer period than fluid on the boundary.

It is useful to consider the theoretical flow generated by an isolated parabolic dome of dense fluid moving along a slope derived by Swaters & Flierl (1991). This model assumes geostrophic flow in the dome and quasi-geostrophic flow in the ambient fluid. The predicted speed of the dome along the slope is c_N. The predicted motion in the ambient fluid is everywhere cyclonic, with a core above the centre of the dense dome that is nearly in solid-body rotation. From our experiments we have estimated the relative rotation of the core of the eddies around the translating eddy centres by observing the motion of individual particles, particle pairs and clouds of powder as they move around the eddies (assuming the core to be in solid-body rotation). The results are presented in figure 11. There is a good deal of scatter in these results, as is to be expected from the rather crude methods used, but there is a clear increase in the strength of the eddy with increasing Γ. The eddies appear to be remarkably strong, with relative vortices of order f (approximately $2f$ for $\Gamma = 0.5$).

4.6. *Injected source*

Some of the flows with the injected source fluid also produced eddies that propagated along the slope. Eddies again occurred when there was sufficient stretching and not too much viscous draining, but the criteria were more restrictive ($\Gamma > 0.09$ and $Y/L > 17.5$). The eddies formed farther downstream of the source in this case than for the weir
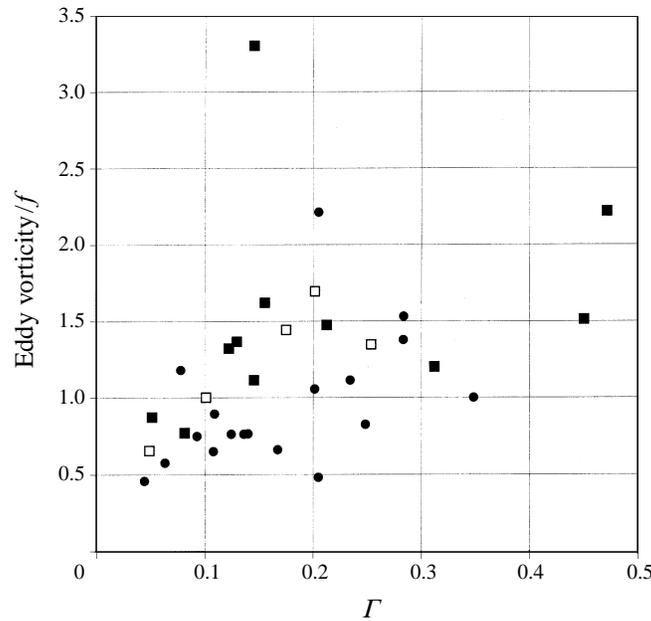
FIGURE 11. The vorticity of the eddies compared with the background vorticity as a function of the stretching parameter. Symbols as figure 5.

flows and this perhaps explains why weaker viscous draining was necessary for the eddies to be observed. When eddies did form, the speed of propagation and the frequency of production followed the same relations as were found for the weir flows (as shown on figures 8 and 9).

4.7. *Alternative scalings*

Finally, we may use our results to test possible mechanisms for eddy production. We discuss two possible mechanisms here, and consider further explanations in the final section.

One may hypothesize that eddies may be produced if the initial flow conditions are such as to satisfy (14), and cause the flow to attempt to set up a bi-directional current (the 'bi-directional hypothesis'). Since there is no source of fluid at the downstream end, the fluid must turn anticyclonically at the nose of the current in order to attempt to simulate bi-directional flow, and eddy formation may result from this nonlinear process. This suggests that (14) should be tested as a criterion for the formation of eddies. The time interval between the observed eddies is shown plotted as a function of s in figure 12(*a*). No discernible pattern is observed, and this suggests that s is not an important parameter for the formation of the eddies observed here. Hence the 'bi-directional hypothesis' is discarded.

Second, Swaters (1991) has carried out a linear stability analysis of steady dense currents on a slope in a stationary homogeneous environment. His governing equations are quasi-geostrophic in the upper layer, but more general in the lower layer where they take into account motion of the boundaries of the dense fluid. The stability properties of this system are governed by the interaction parameter μ defined by equation (15). The analysis produces growing baroclinic disturbances concentrated on the deep side of the current, with the familiar phase differences between the upper and lower layers. Both the growth rate and wavenumber of these disturbances increase with
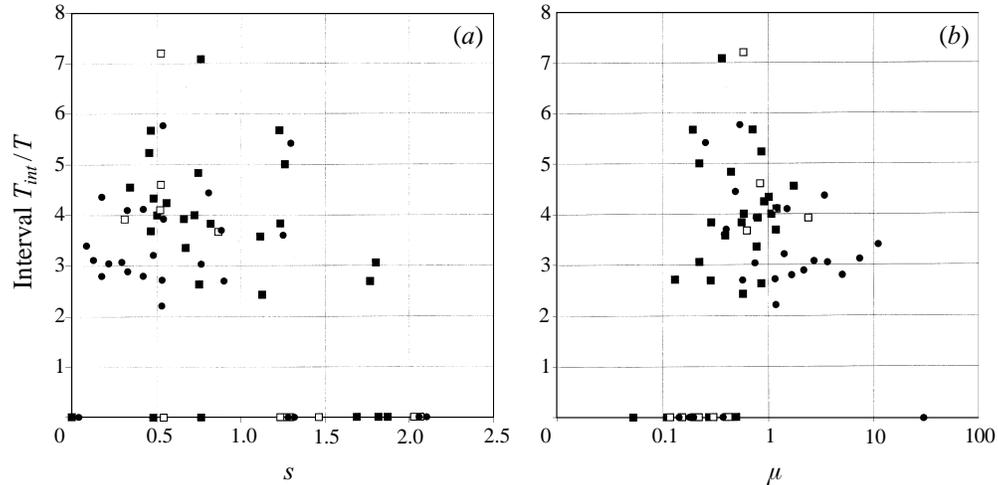
FIGURE 12. The interval between one eddy and the next as a function of (*a*) the scaled slope, *s*, (*b*) Swater's interaction parameter, μ. Symbols as figure 5.

μ, with the phase speed remaining approximately constant. In the present experiments the initial steady current is generally not established, and hence it cannot support eddies produced by this instability process. Nonetheless the relevance of this baroclinic mechanism can be tested by examining the sensitivity of the properties of the observed eddies to μ. Figure 12(*b*) shows the time interval between eddies plotted as a function of μ. Again, there is no discernible relationship, and hence there is no evidence that baroclinic instability is important for the formation of these eddies.

In summary, we conclude that *s* and μ are not relevant scaling parameters for these flow phenomena.

5. Discussion

5.1. *Model for eddy formation*

The quantitative observations described above, together with close scrutiny of the phenomena on the video tapes, suggest the following scenario for eddy formation, in which Ekman drainage plays an important part but baroclinic instability does not. We address specifically the case where the fluid is ejected horizontally along the slope from the source, rather than the flow over the sill, because of its greater simplicity and its amenability to analytical treatment. The observations indicate that the same process for eddy formation applies in both cases. We first give a short overview of this scenario, and then discuss its various stages in more detail.

In brief, the inflowing lower layer suffers a reduction in thickness from two processes: geostrophic adjustment, which occurs on the rotation time scale and causes anticyclonic vorticity in the layer, and Ekman drainage, which occurs on a longer time scale, and does not. Both processes decrease the thickness of the lower layer, and if the fluid in the layer above is relatively static or 'captured' during this reduction, the relative vorticity there will become cyclonic by conservation of potential vorticity. If this process occurs strongly enough (or for a sufficiently long time) in a localized region, a closed eddy forms in the upper layer, which is communicated barotropically to the lower layer by the pressure field. This causes the net Ekman drainage flux to decrease, and the decreased central pressure causes a small convergence in the lower
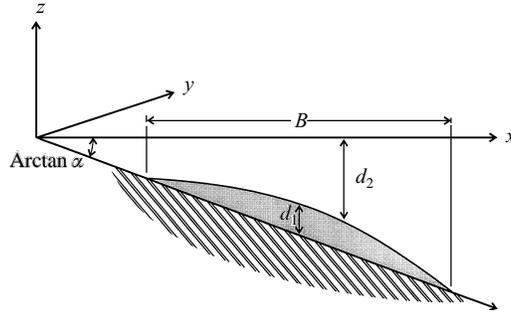
FIGURE 13. Definition sketch for a dense layer on a slope.

layer. The eddy produced then propagates along the slope as a distinct entity, removing the fluid from the generation region and causing the process to begin again. We first describe this sequence of dynamical processes that produces these eddies, and then compare the resulting predictions with the observations.

The observed eddy formation process may be broken down into five stages or processes, some of which operate simultaneously: geostrophic adjustment of the initial flow, Ekman drainage, capture (of the upper-layer fluid by the lower layer), collapse of the lower layer and vortex stretching of the upper layer, and, finally, eddy formation and propagation. We now describe the dynamics of each of these stages in turn.

(i) *Geostrophic adjustment.* The dense fluid is ejected through a nozzle of approximate width B_0, height d_0 and volume flux Q_0, so that the dense flow initially has this width and height. For these experiments we have $d_0 = 1.5$ cm, $B_0 \approx 8$ cm (the shape tapers to zero at ± 5 cm). This flow then adjusts to a state of geostrophic balance within the time scale of a rotation period. This is an inviscid process, and is approximately described by the following equations.

We take Cartesian coordinates with x and y horizontal and z vertical, as shown in figure 13, with u, v and w the velocity components in the directions of x, y and z increasing respectively. The flow of a two-layer fluid in hydrostatic and geostrophic balance, with $u = 0$ everywhere and no alongslope variation, is given by

$$-fv_1 = -g((d_1+d_2)_x - \alpha) + g'd_{2x}, \quad -fv_2 = -g((d_1+d_2)_x - \alpha), \qquad (18)$$

where the suffices 1 and 2 denote the lower and upper layers respectively, so d_1 and d_2 denote the local depth of these layers. The inflowing fluid is assumed to have uniform potential vorticity which may be taken to be f/d_0, and we assume this flows into a fluid at rest. Conservation of potential vorticity in the lower layer then gives

$$\frac{f+v_{1x}}{d_1} = \frac{f}{d_0}, \quad \frac{f+v_{2x}}{d_2} = \frac{f}{D_0-d_0}, \qquad (19)$$

where D_0 is the initial undisturbed total depth above the slope. Assuming that the change in D_0 is small, d_1 satisfies

$$\lambda^2 d_{1xx} - d_1 = -d_0, \qquad (20)$$

where $\lambda^2 = g' d_0 (D-d_0)/Df^2$. If we choose axes so that d_1 vanishes at $x = \pm B/2$ (where B is yet to be determined) then d_1 satisfies

$$d_1(x) = d_0 \left[1 - \frac{\cosh(x/\lambda)}{\cosh(B/2\lambda)} \right]. \qquad (21)$$
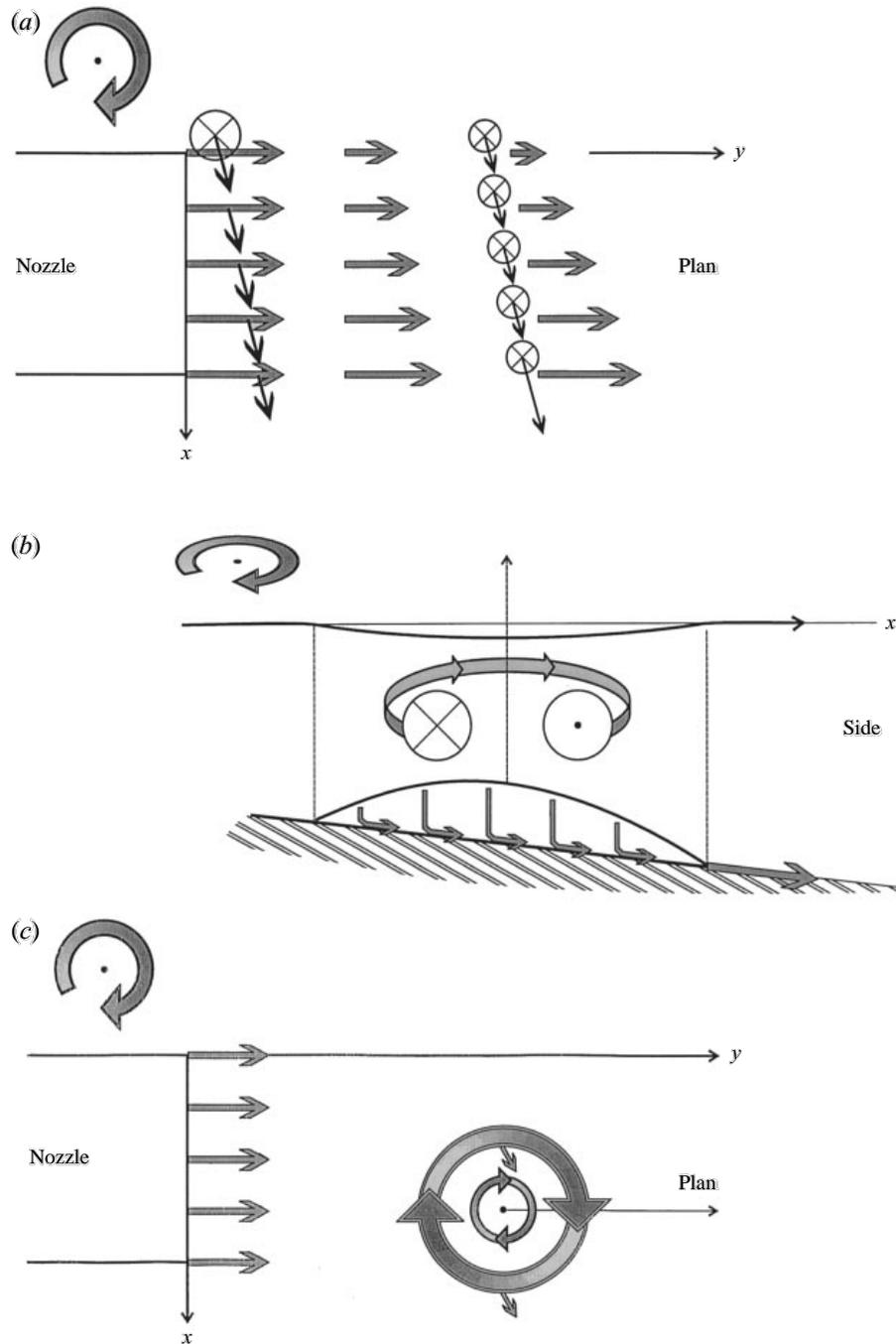
FIGURE 14. Stages in the process of eddy formation. (*a*) Fluid emerges from the nozzle (on the left) and progressively adjusts in the alongslope *y*-direction to geostrophic balance (grey arrows denote alongslope velocity of the dense layer). The black arrows denote flow in the bottom Ekman layer, which is uniform when the current is uniform, but increases in the downslope *x*-direction when geostrophic balance is attained. The arrowtails denote suction of lower-layer fluid into the Ekman layer, due to divergence in the Ekman flux, with size of the arrowtail indicating relative magnitude. (*b*) Spin-up of upper-layer fluid captured over the lower layer, where the latter collapses due to Ekman drainage shown in (*a*). (*c*) The resulting baroclinic eddy has overall cyclonic vorticity, and propagates alongside as a form of finite-amplitude Rossby wave.

Some collapse of the lower layer occurs during this process, as the maximum layer thickness decreases from d_0 to $d_0/\cosh(B/2\lambda)$. This results in an anticyclonic velocity profile given by

$$v_1 = \frac{g'}{|f|}(\alpha - d_{1x}) = \frac{g'}{|f|}\left[\alpha + \frac{d_0}{\lambda}\frac{\sinh(x/\lambda)}{\cosh(B/2\lambda)}\right]. \tag{22}$$

The total fluid flux in this current is

$$Q_0 = \alpha\lambda^2|f|[B - 2\lambda\tanh(B/2\lambda)], \tag{23}$$

so that B increases monotonically with Q_0. B has comparable magnitude to λ in these experiments, and these changes are shown schematically in figure 14(*a*). Equations (18)–(21) then give v_{2x} of order $fd_0/(D_0 - d_0)$ so that geostrophic adjustment alone can generate cyclonic vorticity in the upper layer. This can be substantial if the initial depths of the two layers are comparable, and this probably accounts for the minimum generation period of approximately two rotation periods in figure 9.

(ii) *Ekman drainage.* In the experiment, bottom friction acts on the dense current immediately it exits from the nozzle, and drainage in the Ekman layer occurs coincidentally with the geostrophic adjustment process. Since Ekman layers are generally very thin compared with horizontal scales of motion, it is customary to analyse their vertical structure by neglecting horizontal variations. Equations for such flow on a slope have been described by Nagata *et al.* (1993), and if α is small and the flow is assumed to be steady, they are effectively given by adding νu_{zz} terms to the right-hand side of (18). The behaviour is qualitatively similar to that of the Ekman layer that results from wind stress on the surface of the oceans, and this analogy is helpful in interpreting the behaviour. With the boundary conditions that u_1, v_1 vanish at $z = 0$, and that u and u_z are continuous at $z = d_1$, the local boundary layer solution is

$$u_1 + iv_1 = iv_i[1 - e^{-(1-i)z/d_\nu} - e^{-(1-i)d/d_\nu}\sinh((1-i)z/d_\nu)], \quad 0 < z < d_1, \tag{24}$$

in complex notation, where v_i denotes the inviscid velocity given by (22), and d_ν is the Ekman layer thickness given by (8). From this we may obtain the downslope volume flux Q_E, which is

$$Q_E = \tfrac{3}{4}v_i d_\nu\left[1 + 3\,e^{-2d_1/d_\nu}\sin\left(\frac{2d_1}{d_\nu} + \frac{\pi}{4}\right) - \tfrac{4}{3}e^{-d_1/d_\nu}\sin\left(\frac{d_1}{d_\nu} + \frac{\pi}{4}\right)\right]. \tag{25}$$

This increases approximately linearly from 0 to $3v_i d_\nu/4$ as d_1/d_ν increases from 0 to 3, and then remains approximately unchanged as d_1/d_ν increases further (see Nagata *et al.*, figure 13). This drainage flux is depicted schematically in figure 14(*a*). When (25) is applied to the initial flow (with uniform v_i), it implies that all of the drainage flow emanates from the upslope side of the current, with no divergence in the middle. However, for the geostrophically adjusted current (22) the net drainage is larger, and it is mostly fed by divergence of Q_E, causing downward motion in the current. This Ekman suction velocity w_E is given by

$$w_E = -\frac{dQ_E}{dx} \approx \frac{3d_\nu g'}{4|f|}d_{1xx}, \tag{26}$$

which is negative (downward) in the current and largest at the highest and lowest points (with $\cosh(x/\lambda)$ dependence), and with a magnitude of $O(\nu f)^{1/2}$. Application of

(26) as a lower boundary condition to the inviscid two-layer equations shows that it reduces the thickness of the lower layer, but more strongly at the sides than in the middle. This tends to promote doming in the centre. There is also significant additional drainage from the upslope side of the current (since, as discussed, there is no replenishment from higher up the slope), which depletes the thickness there and further sharpens up the boundary of the dense fluid.

(iii) *Capture*. An essential ingredient in the process is the effect of the collapse (or reduction in thickness due to geostrophic adjustment and Ekman drainage) of the lower layer on the upper-layer fluid. For this to be effective, the upper-layer fluid must be situated above the collapsing layer for a sufficiently long period, and we then say that the upper-layer is 'captured'. If the flow is varying with time, so that the collapse occurs at a fixed location, the upper-layer fluid is captured if it is stationary. If the lower-layer flow is steady and its thickness decreases along the streamlines, the upper-layer fluid is captured if it follow the same path. Fluid in a Taylor column over an obstacle, for example, is captured in the same way.

(iv) *Collapse and vortex stretching*. When the lower layer collapses by sinking into the Ekman layer, its potential vorticity is not conserved. However, captured upper-layer fluid does conserve its potential vorticity in this process, in the form

$$\frac{f+v_{2x}}{d_2} = \frac{f}{D-d_0}. \tag{27}$$

Since $d_1+d_2 \approx D$, as d_1 decreases d_2 must increase, and the upper-layer vorticity becomes cyclonic, from (27) (see figure 14*b*). The small perturbation of the free surface is then given by

$$v_{2x} \approx f\left[\frac{d_2}{D-d_0}-1\right] = \frac{g}{f^2}(d_1+d_2)_{xx}, \tag{28}$$

and from (18) the lower-layer velocity satisfies

$$v_1 = v_2 + \frac{g'}{|f|}d_{2x}. \tag{29}$$

Hence the stretching of the upper layer causes a net cyclonic barotropic motion, and the maximum value attainable depends on the initial fractional depth of the upper layer. This cyclonic barotropic velocity reduces the initial anticyclonic velocity (due to geostrophic adjustment) in the lower layer and this in turn causes a net decrease in the Ekman drainage flow. In the experiments where the dense fluid is released over a sill, it undergoes some net downslope displacement. This also contributes to vortex stretching of the upper layer if the latter is captured. However, this does not occur in experiments with the horizontally released fluid.

(v) *Eddy formation and propagation*. The above discussion and accompanying equations have been two-dimensional, with variation in the *y*-direction suppressed. The processes of capture, collapse and vortex stretching will generally be three-dimensional in practice, but the two-dimensional concepts are readily generalized, and axisymmetric equations have the same form. Vortex stretching in the upper layer will clearly tend to cause a closed vortical circulation there, and this effect will be transmitted to the lower layer by the pressure. The net result will be a baroclinic eddy but with a large barotropic component, cyclonic in the upper layer and relatively anticyclonic in the lower, with a domed interface and much reduced Ekman drainage (shown schematically in figure 14*c*). These eddies are observed to propagate along the slope at a variety of speeds (see figure 8). There does not appear to be a complete theory

for eddies of this type, but there are two dynamical processes that support this propagation. First, geostrophic balance with gravity acting on the blob of dense lower-layer fluid in the eddy gives the speed $g'\alpha/|f|$. This effect is independent of the size of the blob, but should be reduced when the depth of the blob is reduced to the order of the Ekman layer thickness. Secondly, the flow induced by the barotropic component of the eddy itself causes a secondary dipole of barotropic perturbation vorticity (the β-gyres), which causes the vortex to move in the direction of the dipole axis (McWilliams & Flierl 1979; Reznik & Dewar 1994). This speed is also of order $g'\alpha/|f|$, and is primarily alongslope with a small upslope component. Baroclinic components of the vortex produce further complications that have a smaller affect on the speed, but affect the vortex structure in the long term (Reznik, Grimshaw & Sriskandarajah 1996). The resulting eddy speed is the sum of these effects. This is generally consistent with the observed speeds, except that the latter are less than $g'\alpha/|f|$ if damping is sufficiently rapid. Eddies from fluid released alongslope are observed to have a clear upslope component. This eddy propagation removes a substantial body of fluid from the vicinity of the source in the experiments, and enables the eddy generation process to be repeated. The whole process is summarized in figure 14.

Comparison between the above dynamical scenario and the quantitative observations shown in figure 9 and 11 is not straightforward, because of the various processes involved and their different time scales, but some correspondence may be found. Geostrophic adjustment occurs in the time scale of a rotation period. If the collapse during this adjustment is large enough to initiate an eddy, then this will be the generation time, and this limit is reflected in figure 9. If the collapse and spin-up is primarily due to uniform Ekman drainage, the time-scale for spin-up of the upper layer is $(D-d_0)/(\nu f)^{1/2}$, which gives dependence on D and f that is consistent with figure 9. This behaviour is also consistent with the variation of eddy strength shown in figure 11. Ekman drainage from the upslope side of the eddy gives a third time scale, and a fourth comes from the eddy propagation speed $O(g'\alpha/f)$, since the eddy must move at least a diameter before the generation process can be repeated. In practice, of course, these processes and their operating times overlap. It is interesting that viscous drainage can promote eddy generation and propagation by vortex stretching, but also inhibit propagation by removing dense lower-layer fluid.

5.2. *Application to oceanographic flows*

A similar process has recently been identified in a numerical study by Spall & Price (1997), of an idealization of the Denmark Strait overflow, which contains two downslope co-flowing layers. Here, flow of the lower layer causes stretching of the upper layer, and rapid barotropic vortex formation in both, although the forcing conditions are effectively steady. Cyclonic eddies have been observed over the Denmark Strait overflow (e.g. Bruce 1995; Krauss 1996).

The initial motivation for this work was the flow of dense water on slopes in the ocean and so it is useful to see how our work relates to such flows. In order to compare the laboratory flows with oceanographic flows it is necessary to replace the molecular viscosity of the laboratory flows with a vertical eddy viscosity for the oceanographic flows. We do this by matching the stress in a simple viscous boundary layer with the stress estimated by a quadratic drag law,

$$\tau = A_Z c_N/d_A = kU^2, \tag{30}$$

where A_Z is the vertical eddy viscosity, d_A the boundary layer thickness based on this ($d_A = (2A_Z/f)^{1/2}$), U is the velocity scale from the scalings in §3 and k is taken to be

2.5×10^{-3} (a typical value for oceanographic flows, e.g. Lane-Serff 1993, 1995; Bombosch & Jenkins 1995). Equation (30) can be rearranged to give A_Z in terms of known quantities,

$$A_Z = (2k^2 U^4)/(fc_N^2) = (4k^2 Qf^2)/(g'\alpha^2). \tag{31}$$

Thus a flow with a volume flux of $Q = 5 \times 10^6 \text{ m}^3 \text{ s}^{-1}$ (5 Sverdrup) and density difference of 0.05%, flowing onto a slope of $\alpha = 0.02$ at a depth of $D = 1000$ m gives (assuming $f = 10^{-4} \text{ s}^{-1}$),

$$A_Z = 0.64 \text{ m}^2 \text{ s}^{-1}, \quad L = 15 \text{ km}, \quad Y = 45 \text{ km}, \quad Y/L = 3.0, \quad c_N = 0.98 \text{ m s}^{-1}, \quad \Gamma = 0.3.$$

From our results we predict that such a flow would produce eddies with a frequency of one every $(4\pi/f)(0.10/\Gamma + 2.4) = 106$ hours, a radius of $1.25L = 18.8$ km, and the eddies would propagate along the slope a distance $2.3L = 34.5$ km out from the source (where the water is 1690 m deep) at a speed of $0.1 (Y/L)^{0.62} c_N = 0.19 \text{ m s}^{-1}$. While the eddies propagate along the slope there would be a viscous layer draining fluid at an angle down the slope in a layer of thickness scaling with $d_A = 113$ m.

6. Summary

We have shown that a dense current on a slope can generate eddies in the fluid above the current. The eddies are cyclonic and the data shown in figure 9–11 imply that they are generated by vortex stretching in the upper layer, as discussed above. The eddies occur provided that viscous draining is not dominant ($Y/L > 3.5$). The frequency of the eddies depends on Γ, reaching approximately one eddy every two revolutions for Γ larger than 0.3, with the frequency decreasing for smaller Γ. For sufficiently weak stretching ($\Gamma < 0.07$ for our experiments) no eddies could be observed at all. However, this appears to be a feature of our particular experiments, in that they were not of sufficiently long duration for eddies of such low frequencies to be observed. Low frequencies at lower values of Γ have been observed by Smith (1977). The strength of the eddies also depends on Γ, with the eddy vorticity reaching $2f$ for $\Gamma = 0.5$. The eddies move along the slope, with a speed that depends on viscous draining effects and generally scales on c_N (at least for moderate values of Y/L). In contrast, for weak viscous draining (large Y/L), the eddy speed appears to be related to the speed of a rotating current flowing on a horizontal surface, which scales on u. However, it is difficult to separate the effects of a relatively small topographic slope (small s) from weak viscous draining.

Our results can be applied to oceanographic flows, provided the molecular viscosity appropriate in the laboratory flows is replaced by a vertical turbulent eddy viscosity in the oceanographic flow. The simple eddy viscosity method probably overestimates the draining flux but all the input fluid will eventually drain downslope in the viscous flow in any case. It is the behaviour of the viscous layer that determines where the dense flow will leave the slope and flow into the main body of the ocean, and this viscous behaviour is under study. However, the eddy formation discussed in this paper clearly has an influence on the viscous flow as well as a dramatic effect on the flow in the fluid above the dense current.

In many oceanographic situations the stratification of the ambient fluid is significant, and its effects need to be included in order to make detailed comparisons between the oceanographic and laboratory flows. In a sequel to this work we will show how stratification can effectively put a 'lid' on the flow, reducing the effective depth of the overlying fluid (i.e. making D smaller) and thus enhancing vortex stretching and eddy formation.

REFERENCES

BAINES, P. G. 1998 Downslope flows into a stratified environment – structure and detrainment. In *Mixing and Dispersion in Stably Stratified Fluids. Proc. 5th IMA Conf. on Stratified Flows, Dundee*. IMA (to appear).

BAINES, P. G. & CONDIE, S. A. 1998 Observations and modelling of Antarctic downslope flows. In *Oceanology of the Continental Shelf* (ed. S. S. Jacobs & R. Weiss), American Geophysical Union (to appear).

BOMBOSCH, A. & JENKINS, A. 1995 Modeling the formation and deposition of frazil ice beneath Filchner-Ronne Ice Shelf. *J. Geophys. Res.* **100**, 6983–6992.

BRUCE, J. G. 1995 Eddies southwest of the Denmark Strait. *Deep-Sea Res.* I **42**, 13–29.

CONDIE, S. A. 1995 Descent of dense water masses along continental slopes. *J. Mar. Res.* **53**, 897–928.

GRIFFITHS, R. W. 1986 Gravity currents in rotating systems. *Ann. Rev. Fluid Mech.* **18**, 59–89.

GRIFFITHS, R. W. & HOPFINGER, E. J. 1983 Gravity current moving along a lateral boundary in a rotating fluid. *J. Fluid Mech.* **134**, 357–399.

GRIFFITHS, R. W., KILLWORTH, P. D. & STERN, M. E. 1982 Ageostrophic instability of ocean currents. *J. Fluid Mech.* **117**, 343–377.

HARVEY, L. D. D. 1996 Polar boundary layer plumes and bottom water formation: A missing element in ocean general circulation models. *J. Geophys. Res.* **101**, 20799–20808.

JENKINS, A. 1991 A one-dimensional model of ice shelf-ocean interaction. *J. Geophys. Res.* **96**, 20671–20677.

KARSTEN, R. H. & SWATERS, G. E. 1996 Nonlinear stability of baroclinic fronts in a channel with variable topography. *Stud. Appl. Maths* **96**, 183–199.

KILLWORTH, P. D. 1977 Mixing on the Weddell Sea continental slope. *Deep-Sea Res.* **24**, 427–448.

KRAUSS, W. 1996 A note on overflow eddies. *Deep-Sea Res.* I **43**, 1661–1667.

LANE-SERFF, G. F. 1993 On drag-limited gravity currents. *Deep-Sea Res.* I **40**, 1699–1702.

LANE-SERFF, G. F. 1995 On meltwater under ice-shelves. *J. Geophys. Res.* **100**, 6961–6965.

MCWILLIAMS, J. C. & FLIERL, G. R. 1979 On the evolution of isolated, nonlinear vortices. *J. Phys. Oceanogr.* **9**, 1155–1182.

MORY, M., STERN,, M. E. & GRIFFITHS, R. W. 1987 Coherent baroclinic eddies on a sloping bottom. *J. Fluid Mech.* **183**, 45–62.

NAGATA, Y., KIMURA, R., HONJI, H., YAMAZAKI, Y., KAWAGUCHI, K. & HOSOYAMADA, T. 1993 Laboratory experiments of dense water descending on continental slope. In *Deep Ocean Circulation, Physical and Chemical Aspects* (ed. T. Teramoto), pp. 333–350. Elsevier.

PRICE, J. F. & BARINGER, M. O'N. 1994 Outflows and deep water production by marginal seas. *Prog. Oceanogr.* **33**, 161–200.

REZNIK, G. M. & DEWAR, W. K. 1994 An analytical theory of distributed axisymmetric barotropic vortices on the β-plane. *J. Fluid Mech.* **269**, 301–321.

REZNIK, G. M., GRIMSHAW, R. H. J. & SRISKANDARAJAH, K. 1996 On basic mechanisms governing the evolution of two-layer localised quasigeostrophic vortices on a β-plane. *Monash Univ. Dept. of Mathematics Rep.* 96/36.

SMITH, P. C. 1975 A streamtube model for bottom boundary currents in the ocean. *Deep-Sea Res.* **22**, 853–873.

SMITH, P. C. 1977 Experiments with viscous source flows in rotating systems. *Dyn. Atmos. Oceans* **1**, 241–272.

SPALL, M. A. & PRICE, J. F. 1998 Mesoscale variability in Denmark Strait: the PV outflow hypothesis. *J. Phys. Oceanogr.* (in press).

SWATERS, G. E. 1991 On the baroclinic instability of cold-core coupled density fronts on a sloping continental shelf. *J. Fluid Mech.* **224**, 361–382.

SWATERS, G. E. 1993*a* On the baroclinic dynamics, Hamiltonian formulation and general stability characteristics of density-driven surface currents and fronts over a sloping continental shelf. *Proc. R. Soc. Lond.* A **345**, 295–325.

SWATERS, G. E. 1993*b* Nonlinear stability of intermediate baroclinic flow on a sloping bottom. *Proc. R. Soc. Lond.* A **442**, 249–272.

SWATERS, G. E. & FLIERL, G. R. 1991 Dynamics of ventilated coherent cold core eddies on a sloping bottom. *J. Fluid Mech.* **223**, 565–587.

WHITEHEAD, J. A., STERN, M. E., FLIERL, G. R. & KLINGE, B. A. 1990 Experimental observation of baroclinic eddies on a sloping bottom. *J. Geophys. Res.* **95** (C6), 9585–9610.

ZATSEPIN, A. G., KOSTYANOI, A. G. & SEMENOV, A. V. 1996 An axisymmetric density current over a sloping bottom in a rotating fluid. *Oceanology* (*Engng Trans.*) **36**, 311–316.